Biochemical and Biophysical Research Communications 463 (2015) 496–503

Contents lists available at ScienceDirect

Biochemical and Biophysical Research Communications

journal homepage: www.elsevier.com/locate/ybbrc

Equilibrium dissociation and unfolding of human papillomavirus E2 transactivation domain

Nitu Singh, Shruthi Kanthaje [1], Kakoli Bose*

Integrated Biophysics and Structural Biology Lab, ACTREC, Tata Memorial Centre, Navi Mumbai 410210, India

ARTICLE INFO

Article history:
Received 23 April 2015
Accepted 14 May 2015
Available online 16 June 2015

Keywords:
HPV
E2
Dimer
Equilibrium
Thermodynamic
Unfolding

ABSTRACT

Papillomavirus E2 protein that performs essential functions such as viral oncogene expression and replication represents specific target for therapeutic intervention. DNA-binding activity is associated with its C-terminal DNA-binding domain (DBD), while the N-terminal transactivation domain (TAD) is responsible for replication and transactivation functions. Although both demonstrate large dependence on dimerization for mediating their functions, K_D for N-terminal dimerization is significantly high suggesting more dynamic role of this domain. However, unlike DBD, very little information is available on TAD dimerization, its folding and stability. Therefore, with an aim at delineating the regulatory switch of its dimerization, we have characterized high-risk HPV18 E2 TAD. Our studies demonstrate that E2 TAD is a weak but thermodynamically stable dimer (K_D ~ 1.8 μM, ΔG^{H_2O} = 18.8 kcal mol^{-1}) with α2–α3 helices forming the interface. It follows a three-state folding pathway, in which unfolding involves dissociation of a dimeric intermediate. Interestingly, 90% of the conformational free energy is associated with dimer dissociation (16.9 of 18.8 kcal mol^{-1}) suggesting dimerization significantly contributes to its overall thermodynamic stability. These revelations might be important toward designing inhibitors for targeting dimerization or folding intermediates and hence multiple functions that E2 performs.

1. Introduction

Human papillomaviruses (HPVs) are double-stranded DNA viruses that have been strongly implicated in development of lesions ranging from skin or genital warts to cancer [1]. Based upon oncogenicity, they are divided into two subclasses, high-risk (HR) types including HPV16 or 18 that are associated with 70% cases of cervical cancer, and benign wart-causing low risk (LR) types such as HPV6 and 11. Tremendous divergence in pathogenesis of HPVs has evolved due to complex system of regulation mediated by protein-DNA and protein–protein interactions between viral and host factors [2]. Particularly, the early protein E2 acts as a master regulator of the viral life-cycle. While considered to be the principal transcription factor, the E2 protein is equally important for viral DNA replication as well as mitotic partitioning of the viral genome [3]. In addition, several groups have demonstrated myriads of other functions such as NFκB activation [4], induction of apoptosis [5] or regulation of host cell cycle [6]. The correlation of E2 with mechanisms linked with cellular transformation hypothesizes its direct involvement in early steps of carcinogenesis, and thus exemplifies it as a potent target for therapeutic intervention.

E2 proteins characterized from numerous human and animal serotypes have three distinct modules; an amino-terminal transactivation domain (TAD) followed by a flexible, proline-rich hinge region and a carboxyl-terminal DNA-binding domain (DBD). TAD is a protein–protein interaction domain that binds to the viral helicase E1 [7] and to various host proteins such as topoisomerase-I [2], Brd4 [8] and procaspase-8 [5]. Crystal structures of TAD reveal that it comprises two sub-domains, N1 and N2, packed antiparallel to one another and separated by two consecutive single helical turns [7,9,10]. Although the main dimerization interface is located within DBD, which strongly dimerizes (nanomolar K_D) and tightly binds to viral DNA sites [11], available structures suggest that TAD also homodimerizes, however, with a higher K_D [9,12]. Dimerization of TAD has been proposed to serve as a molecular switch between early gene expression and viral genome replication during HPV infection [9,13]. Studies have also shown that induction of apoptosis by HPV16 E2 requires formation of functional TAD dimers, thereby further emphasizing the requisite for dimerization [14]. For HPV16 E2, the dimerization of TAD involves residues from helices α2/α3 of

* Corresponding author.
E-mail address: kbose@actrec.gov.in (K. Bose).
[1] Present address: PGIMER, Chandigarh 160012, India.

http://dx.doi.org/10.1016/j.bbrc.2015.05.057
0006-291X/

N1 and 142–144 from N2 domains [9]. Nonetheless, with respect to HR-HPV18 E2, the possibility of TAD dimerization is still obscure. The available crystal structure has 65 N-terminal residues (two-thirds of N1 domain) missing and therefore lacks key amino acids reported for dimerization [15]. Furthermore, despite numerous reports on the biophysical properties of DBD, till date, no information is available on TAD folding and stability. A precise understanding of folding as well as determination of the overall conformational stability will help delineate the regulatory switch for E2 TAD dimerization which is crucial to understand its biological functions.

Here, using molecular modeling, mutagenesis and biophysicochemical approaches, we distinctly show that HR-HPV18 E2 TAD dimerizes at micromolar concentration. The dimerization is mediated by R41 and W42 as opposed to a single key residue R37 reported for HPV16 E2 [13]. In addition, we provide the first evidence on unfolding and conformational stability of E2 TAD.

2. Materials and methods

2.1. Molecular modeling, docking and simulation

Using Modeller-9v11 [16], the missing region of HPV18 E2 TAD (PDB: 1QQH) was homology modeled using HPV16 E2 TAD (PDB: 1DTO) as a template [9]. To obtain TAD dimer, the modeled monomeric HPV18 E2 TAD was superimposed on dimeric HPV16 E2 TAD, having C2 biological symmetry, using PyMol (Schrödinger, LLC). To verify correct assembly of dimeric interface, molecular docking of the monomer was performed with ClusPro-2.0 [17]. The final structure was energy minimized with PRIME Minimization module (Schrödinger, LLC) and further subjected to molecular dynamic simulation for 20 ns as described previously [18]. The simulated models were verified and validated using PROCHECK [19], ProSA-web [20], and ERRAT algorithms [21].

2.2. Sub-cloning, protein expression and purification

pEGFPc1-HPV18 E2 vector was a kind gift from Dr. F. Thierry (Institute of Medical Biology, Singapore). E2 TAD (residues 1–201) was sub-cloned in pACYC-vector (Clontech), and a C-terminal his_6-tag was introduced to facilitate protein purification. Mutants were generated using site-directed mutagenesis kit (Stratagene) and verified by DNA sequencing. *Escherichia coli* BL21(DE3) cells transformed with TAD constructs were grown at 37 °C till the $O.D_{600}$ reached 0.5, further induced with 2 μg/ml of arabinose and cultured at 18 °C for 20 h. The Ni^{+2}-affinity purification was performed in buffer-A (10 mM Na_2HPO_4/NaH_2PO_4, pH 7.5, 100 mM NaCl, 20 mM β-mercaptoethanol) as described previously [22]. The proteins were further purified and characterized by size exclusion chromatography using Superdex200-10/30 column (GE Healthcare). Protein identity was confirmed with Western blotting using anti-E2 antibody (sc-26939).

2.3. Glutaraldehyde cross-linking

20 μg of purified protein was treated with freshly prepared glutaraldehyde solution (final concentration 0.1%) for 2 min at 37 °C. The reaction was terminated by adding 5 μl of 2 M Tris–HCl, pH 8.0. Cross-linked product was mixed with Laemmli sample buffer and analyzed on 12% SDS-PAGE.

2.4. Dynamic light scattering (DLS)

1 mg/ml protein was loaded into a 45 μl quartz cuvette. Measurements were performed at 25 °C and at least 10 scans each of 12 s duration were collected (DynaPro NanoStar, Wyatt Technology). Histogram analyses were carried out using DYNAMICS v.6.0 software.

2.5. Fluorescence and circular dichroism (CD) spectroscopy

Protein sample preparations for equilibrium unfolding studies were done as described previously [23]. Fluorescence measurements were recorded on Fluorolog-3 spectrofluorometer (Horiba Scientific) with 280 and 295 nm excitation followed by emission between 310 and 400 nm. Far UV CD spectra were acquired using JASCO J-815 spectropolarimeter between 250 and 200 nm, at 20 nm/min scan speed.

2.6. Analysis of the equilibrium unfolding profile

E2 TAD wild-type and single mutants followed a three-state folding pathway with the formation of a dimeric intermediate, $N_2 \rightleftharpoons I_2 \rightleftharpoons 2U$. The data was normalized and fitted to the equations described earlier [23], for obtaining the thermodynamic parameters using Igor Pro 6.03A (WaveMetrics). The data for E2 TAD double mutant was fitted to a two-state monomeric model, $N \rightleftharpoons U$ [23].

3. Results

3.1. In silico analysis of E2 TAD dimerization

To assess homodimerization of HPV18 E2 TAD, a structural model was generated and its overall quality factor was assessed by ERRAT, which was found to be 82% implying good accuracy of the predicted structure. The stereochemical analysis revealed 100% of residues were in the most favorable and additional allowed regions of the Ramachandran plot (Fig. S1A). ProSA-web evaluation provided a compatible Z score value of −7.9 (Fig. S1B), which is well within the range of native conformations of crystal structures. The overall residue energies of the 3D model were largely found to be negative (Fig. S1C). These observations indicated that the model quality was reliable and could be considered for further analysis.

Superposition of HPV16 and 18 E2 TAD dimers showed an RMSD of less than 0.8 Å, suggesting similar conformation for the complexes (Fig. 1A). HPV18 E2 TAD dimer had 1806 $Å^2$ of buried surface area, comparable to the 2026 $Å^2$ reported for HPV16 E2 [9]. At the dimer interface, each subunit primarily contributed residues R41, W42, F48, I77, M81, Q84, Q88 from helices α2 and α3 (Table S1). Notably, residues R41, W42 (helix α2) and Q84, Q88 (helix α3) seem to play central roles in stabilizing the dimer interface (Fig. 1B). Dimerization studies on HPV16 E2 TAD demonstrated that substitution of R37 (equivalent to R41 of HPV18) abolished dimer formation [2]. The residue R41 is preserved while W42 is conserved in terms of its hydrophobicity across different papillomavirus types (Fig. S2). Thus, based on these observations, R41 and W42 of HPV18 E2 TAD were targeted for mutagenesis and further characterization.

3.2. In vitro characterization of wild-type and mutant E2 TAD

To determine whether HPV18 E2 TAD forms dimer in solution, we tested the wild-type and α2 helix mutants (R41A, W42A, and R41A/W42A) for their ability to homodimerize *in vitro*. As the first step, the purity of the proteins was checked on SDS-PAGE and the identity was confirmed with Western blotting using anti-E2 antibody (Fig. S3). The gel filtration profile for E2 TAD variants is presented in Fig. 1C. It shows that the wild-type and mutant proteins exist predominantly as monomers, however, except for the double mutant, a peak corresponding to the dimer is also observed (at a

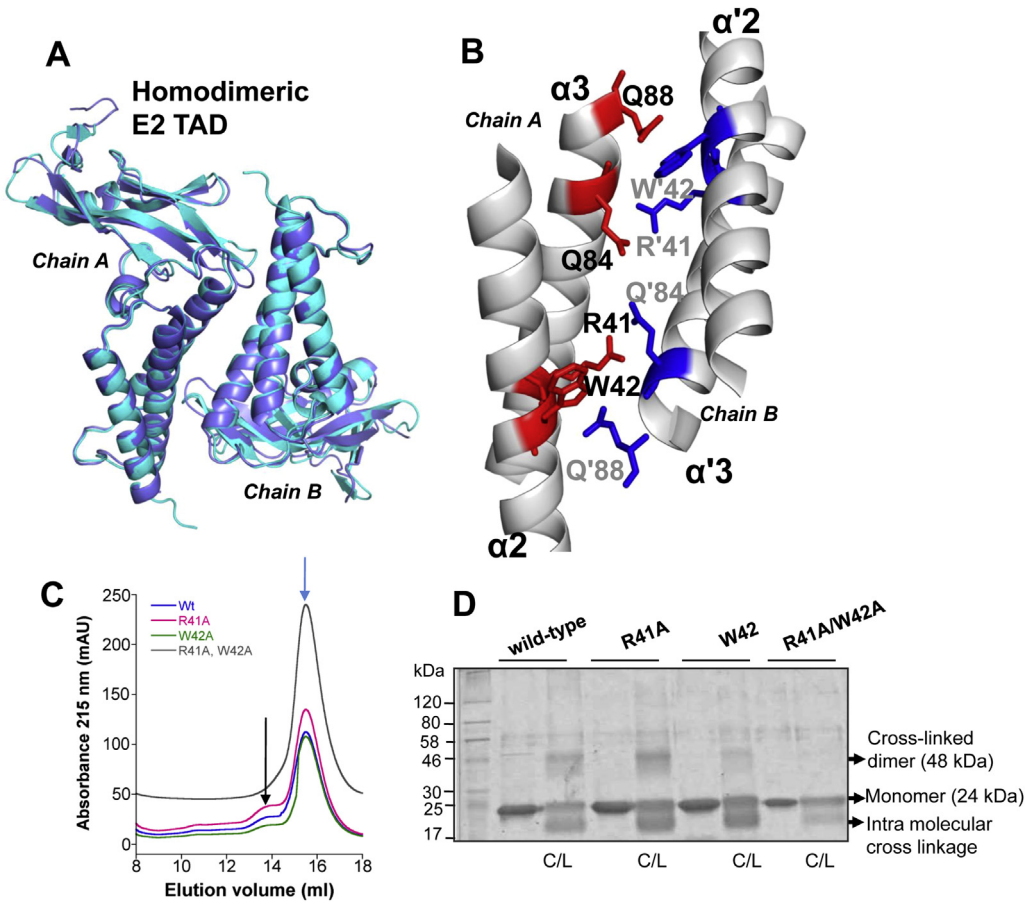

Fig. 1. *In silico* and *in vitro* characterization of HPV18 E2 TAD. A) Superposition of HPV18 and 16 E2 TAD shown in cyan and blue respectively. B) A close-up view of the interface with selected side chains from chain A and B in red and blue respectively. C) Size exclusion chromatography for E2 TAD variants at protein concentrations <10 μM. A major peak (blue arrow) corresponding to the calculated molecular weight of a monomer (24.5 kDa) and a minor peak (black arrow), except for the double mutant, related to the dimeric species (49 kDa) are observed. D) Glutaraldehyde cross-linking reaction product resolved on SDS-PAGE. A band corresponding to size lower than 24 kDa in the cross-linked lane is due to intra-molecular protein cross-linking resulting in increased mobility. C/L represents cross-linked.

final eluant concentration of ~1 μM) suggesting TAD forms a weak dimer. To confirm the presence of the dimeric species, 20 μg of wild-type and mutant proteins were cross-linked with glutaraldehyde and run on SDS-PAGE. The wild-type and single mutants show mixture of monomeric and dimeric species, however, the double mutant was found to exist only in the monomeric form (Fig. 1D). These results demonstrate that at low protein concentrations, TAD wild-type and single mutants are present in monomer–dimer equilibrium.

To substantiate these findings, we determined the heterogeneity of the proteins at higher concentrations (1 mg/ml) using DLS. We observed that the average hydrodynamic radii of TAD wild-type and single mutants were larger compared to the double mutant (Fig. S4). Based upon the radii, the calculated molecular weight of the proteins is given in Table 1. For wild-type and single mutants, the calculated molecular weight closely resembled the theoretical molecular weight of a dimeric E2 TAD, whereas the double mutant showed a homogenous monomeric population.

3.3. Urea-dependent unfolding of E2 TAD

Equilibrium unfolding studies provide an excellent tool to delineate protein stability and determine whether dimerization is a folding event [24]. We therefore studied unfolding of E2 TAD as a function of urea concentration using different spectroscopic probes. In case of wild-type TAD, the data show a first step of unfolding which occurs between 0 and ~2.5 M urea, followed by a second transition between ~3 and 8 M urea. All the three spectroscopic signals showed similar trends in the unfolding (Fig. 2A). To examine reversibility, the protein unfolded in buffer containing 8 M urea was diluted to final urea concentrations shown in Fig. 2A. The data suggest that the folding transitions are completely reversible. Similar experiments were performed with TAD single and double mutant proteins. For both R41A and W42A single mutants, a clear biphasic denaturation curve with reversible folding was observed (Fig. 2B and C). Interestingly, in case of TAD double mutant (R41A/W42A), the data showed only a single reversible transition. A pre-transition occurs between 0 and ~1 M urea which is followed by a cooperative decrease in signal with a post transition baseline between ~5 and 8 M urea (Fig. 2D).

Overall, these results demonstrate that E2 TAD wild-type and single mutants, follow a three-state pathway in which a folding intermediate is in equilibrium with the native and unfolded states. However, strikingly, the double mutant (R41A/W42A) seems to undergo a two-state folding process.

3.4. Protein concentration dependence of unfolding

The mechanism by which oligomeric proteins unfold can be delineated by monitoring the profile of each equilibrium denaturation and its protein concentration dependence. Since E2 TAD homodimerizes, we determined the concentration dependence of

Table 1
Dynamic light scattering analysis of E2 TAD variants.

E2 TAD	Hydrodynamic radius[a]	% Polydispersity[b]	Calculated mean residual molecular weight (kDa)	Theoretical molecular weight (expasy protparam) (kDa)	
				Monomer	Dimer
Wild-type	2.98	34.9	55.4	24.2	48.4
R41A	2.93	31.3	52.7	24.1	48.2
W42A	2.90	18.4	51.1	24.1	48.2
R41A, W42A	2.42	4.5	26.2	24.0	48.0

[a] Mean hydrodynamic radius derived from the measured translational diffusion coefficient using the Stokes–Einstein equation.
[b] Polydispersity divided by the hydrodynamic radius.

the unfolding process. As shown in Fig. 3A–C, there is a shift in the midpoint of the second transition with the increase in protein concentration. However, the first transition is concentration independent and the $U_{1/2}$ value (concentration of urea at which 50% of the protein is unfolded) remains constant. This pattern is consistent with a scheme where a native dimer (N_2) partially unfolds to a dimeric intermediate (I_2), which then unfolds to denatured monomer (2U), $N_2 \rightleftharpoons I_2 \rightleftharpoons 2U$. Thus, fitting of the data to a three-state folding model with a dimeric intermediate was carried out to obtain the conformational free energies (ΔG^{H_2O}) and the co-operativity indices, or *m*-values (Table 2). The data show that the initial unfolding step ($N_2 \rightleftharpoons I_2$) has a $\Delta G_1^{H_2O}$ of <3 kcal mol^{-1}. Thus, the majority of E2 TAD stability resides in its dimerization ($I_2 \rightleftharpoons 2U$), which requires an additional ~17 kcal mol^{-1} to unfold.

By using ΔG^{H_2O} and *m*-values, we calculated equilibrium distribution of the species for all the protein concentrations. As shown in Fig. 4A, between 0 and 3.5 M urea, there is decrease in the population of native dimer with concomitant increase in the population of the dimeric intermediate. The mid-point of the transition is 1.8 M urea that is consistent with the experimental results shown in Fig. 3A. The relative concentration of the dimeric species is dependent on the protein concentration and reaches a maximum at ~3.1 M urea. The second transition, I_2 to U, has midpoint values of 4.3, 4.7 and 4.9 M for the concentration of the proteins indicated in the figure legend. By observing this second-order transition, both as a function of denaturant and protein concentration, we calculated an apparent K_D (K_D^{app}) for the dissociation using equation, $\Delta G_2^{H_2O} = -RT\ln K_D^{app}$. The calculated K_D^{app} at 4.5 M urea was found to be ~1.8 μM which is in close agreement with the dissociation constant K_D, 8.1 ± 4.2 × 10^{-6} M reported for HPV16 E2 TAD dimer [9]. Similar pattern for distribution of three species (native, intermediate, and unfolded) is observed for dimeric R41A and W42A single mutants as shown in Fig. 4B and C.

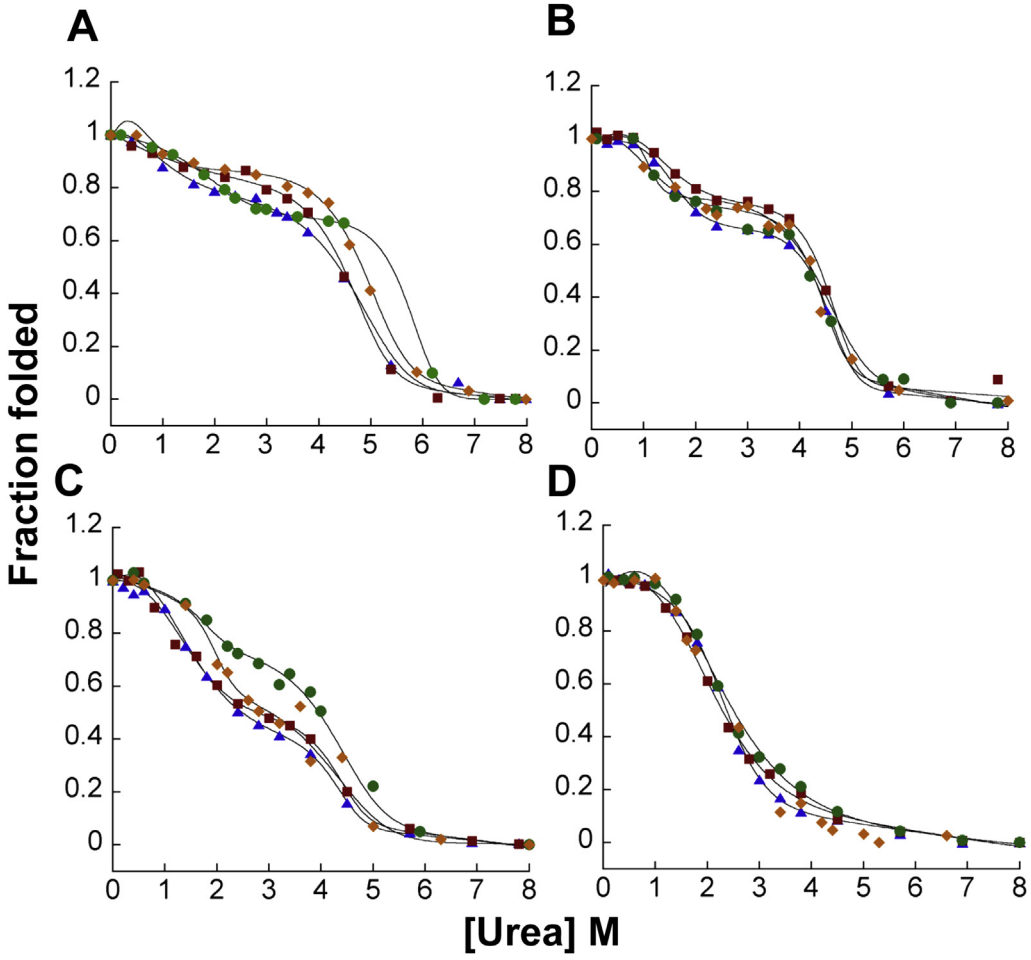

Fig. 2. Equilibrium unfolding of E2 TAD variants. Unfolding measured by fluorescence emission with excitation at 280 (▲), or 295 nm (◆), CD at 228 nm (●) and refolding measured by fluorescence emission with excitation at 280 nm (■). For fluorescence and CD measurements, the protein concentrations were 2.5 μM and 5 μM respectively. For clarity, error bars and refolding data are not shown for all the three data sets. The solid lines represent fit using a three-state (A–C) or two-state folding model (D).

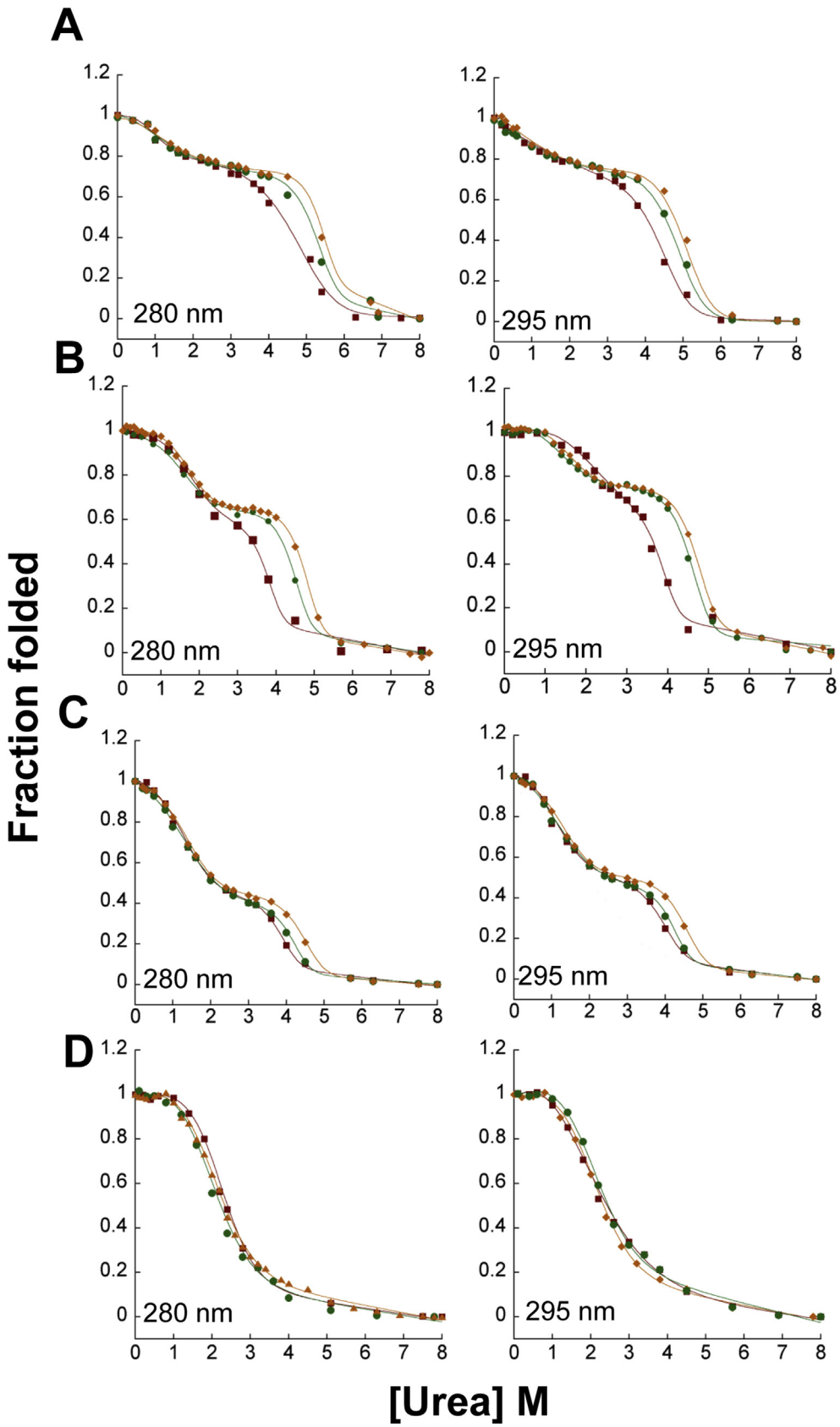

Fig. 3. Protein concentration dependence of unfolding. Equilibrium unfolding monitored by fluorescence emission with excitation at 280 and 295 nm for TAD wild-type (A), R41A (B), W42A (C), and R41A/W42A (D) proteins. The protein concentrations are 1.5, 2.5, and 3.5 μM, each represented by symbols ■, ●, ◆ respectively. The solid lines represent global fits of the data using Igor Pro. For clarity, error bars are not shown for all the data sets.

Table 2
Thermodynamic parameters for E2 TAD wild-type and single mutants.

E2 TAD	m_1 ($N_2 \rightleftharpoons I_2$) (kcal mol^{-1} M^{-1})	m_2 ($I_2 \rightleftharpoons 2U$) (kcal mol^{-1} M^{-1})	$\Delta G_1^{H_2O}$ ($N_2 \rightleftharpoons I_2$) (kcal mol^{-1})	$\Delta G_2^{H_2O}$ ($I_2 \rightleftharpoons 2U$) (kcal mol^{-1})
WT	0.98 ± 0.1	1.97 ± 0.06	1.98 ± 0.1	16.9 ± 0.1
R41A	1.81 ± 0.1	2.39 ± 0.1	2.62 ± 0.6	18.2 ± 0.7
W42A	1.32 ± 0.1	2.18 ± 0.2	2.11 ± 0.2	17.3 ± 0.9

Each entry corresponds to the mean ± S.E. (standard error) of three independent experiments at three different concentrations of the protein: 1.5, 2.5, and 3.5 μM.

We also performed equilibrium denaturation experiments with several protein concentrations of R41A/W42A double mutant. Interestingly, a single sharp transition with no protein concentration dependence is observed between native and denatured states demonstrating that the protein exists as a monomer (Fig. 3D). The total free energy was therefore calculated by fitting the data to a two-state equilibrium model for monomeric proteins. The $U_{1/2}$ and *m*-value of the transition are 2.5 ± 0.1 M urea and 1.4 ± 0.08 kcal mol^{-1} M^{-1}, respectively. The ΔG^{H_2O} ($N \rightleftharpoons U$) of this monomeric variant is thus barely 3.3 ± 0.3 kcal mol^{-1} ($\Delta G^{H_2O} = m[U_{1/2}]$). This stability is similar to the initial unfolding of the dimeric E2 TAD (Table 2). The fraction of species at different urea concentrations is shown in Fig. 4D. Overall, these results suggest that the stability of the dimer contributes significantly to the conformational free energy of E2 TAD protein.

4. Discussion

The results presented here highlight four key properties of HPV18 E2 TAD. Firstly, it is a weak dimer (K_D ~1.8 μM) that readily isomerizes with a lesser cooperativity compared to the second transition, to a partially unfolded dimeric intermediate. Second, presence of a dimeric intermediate suggests dimerization is a folding event. Third, dimerization contributes significantly towards stability of the protein (>89%). Lastly, monomeric TAD variant is substantially destabilized compared to the dimeric protein and unfolds via a two-state pathway without any significantly populated intermediate at the given concentrations.

The biphasic nature of HPV18 E2 TAD denaturation curve and protein concentration-dependent second transition is consistent with the existence of a dimeric intermediate. The overall free energy change involved in the transition from native dimer to the intermediate corresponds to only ~10% of the total stabilization energy (Table 2). However, the second part of the transition is characterized by 8–9 times larger values of $\Delta G_2^{H_2O}$. Moreover, based on the *m*-values ($m_1 << m_2$), the first transition ($N_2 \rightleftharpoons I_2$) shows lack of co-operative unfolding highlighting that the structure is particularly flexible and can easily adopt partially unfolded conformations. Several regions of E2 TAD modular structure, in particular, unstructured key joints and exposed loops at the surface might provide such flexibility [9,15,25]. Preferential interactions of the denaturant with these external regions can be the principal reason

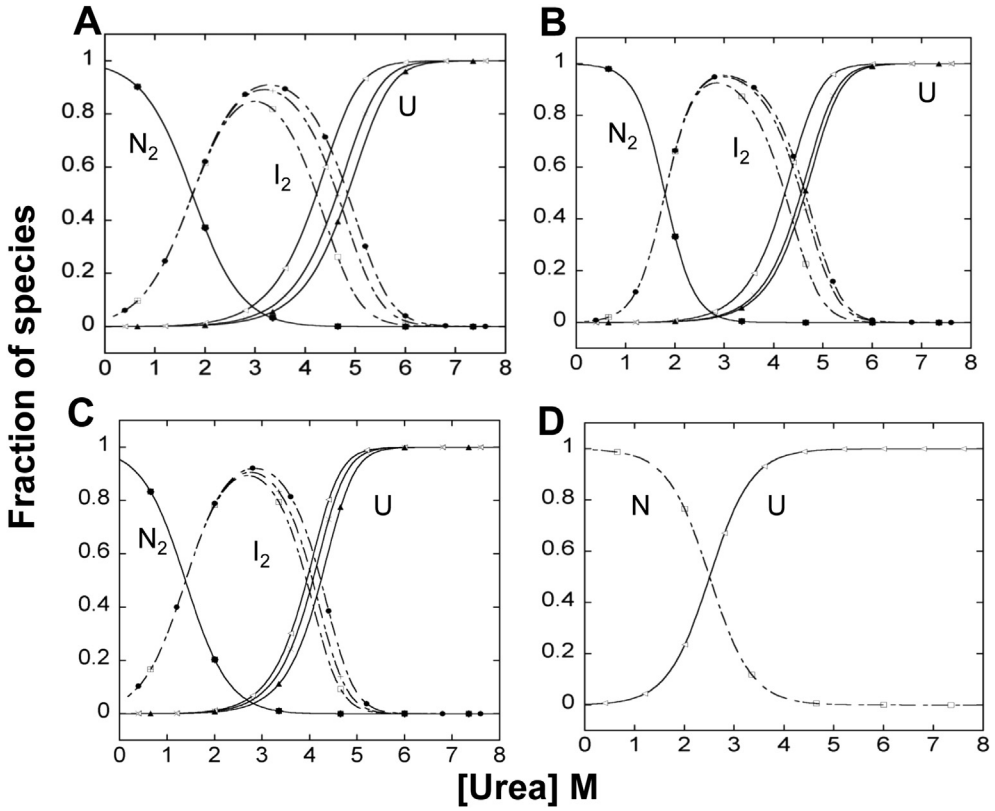

Fig. 4. Fraction of species in the unfolding process. The fraction of native, intermediate and unfolded protein calculated as a function of urea concentration for wild-type (A), R41A (B), W42A (C), and R41A/W42A (D). The protein concentrations are 1.5, 2.5 and 3.5 μM, and N_2 and N refers to the native protein, I_2 is the dimeric intermediate and U refers to the unfolded species.

for local unfolding of the E2 TAD structure far from the dimeric interface.

Denaturant *m*-values can be related to the global changes in accessible surface area (ΔASA) of the protein exposed to solvent during unfolding [26]. Scholtz and co-workers [27] have described empirical relationships that correlate ΔASA with experimental *m*-values, given as, $y = 368 + 0.11(\Delta ASA)$. Using this equation and the *m*-values for E2 TAD wild-type (Table 2), the calculated ΔASAs for the first and second transitions are 5500 $Å^2$ and 14,500 $Å^2$, respectively. This is in agreement with our finding that subunit dissociation and conversion of the intermediate to unfolded E2 TAD monomers occur in second transition, where maximum surface exposure would be expected.

Our data show that HPV18 E2 TAD is reasonably stable with a total free energy change of 18.8 kcal mol^{-1} that is comparable with other dimeric proteins of similar size [28]. Studies on the stability of dimeric and monomeric proteins highlight that the former are, on an average, 4–15 kcal mol^{-1} more stable than the later [24]. Increased stability in case of dimers seems to occur due to burial of additional surfaces upon subunit association [29]. Consistent to this, the monomeric E2 TAD shows a dramatic decrease in the conformational stability. These results demonstrate that the interfacial residues are critically involved in structural stability. Furthermore, both the residues R41 and W42 seem to be crucial for homodimerization, unlike HPV16 E2, where R37A mutation alone resulted in dimer destabilization. Based upon HPV16 E2 TAD dimer structure (PDB ID: 1DTO) and our model for HPV18 E2 TAD, we understand that the possible difference could be due to the type of interactions at the interface (Tables S1 and S2). In HPV16 E2, R37 makes extensive hydrogen bonding and ionic interactions with E80 to stabilize the symmetrical dimer interface. However, in HPV18 E2, E80 is replaced with Q84 which although makes hydrogen contact with R41, does not participate in forming a stabilizing salt-bridge. The additional hydrogen bonds between side chains of W42 and Q88 might be required to provide stability to the dimer interface. Thus, although E2 TAD shares homologous native conformation, the residues and interactions at dimer interface might not be conserved. In support of this observation, recently, studies on BPV1 E2 TAD demonstrated that the dimerization is mediated through redox interactions involving different residues [12,30]. Therefore, while the native structures of E2 are highly conserved, the folding pathways and the intermediates may differ.

In HPV E2 proteins, the extended (~80 amino acids) linker between DBD and TAD provides flexibility to both the domains so as to enable them to function independently [31]. Based on our results, we hypothesize that at lower concentrations, the monomeric TAD species will be populated, which would dimerize only beyond a threshold micromolar concentration. Although E2 is present in a dimeric form even at lower concentrations (mediated by DBD), the more dynamic N-terminal TAD might exist in a monomer–dimer equilibrium. Post viral replication, when the concentration of this protein considerably increases within the host cell, TAD dimerizes through its critical residues which might be a prerequisite for transactivating E6 and E7 oncogenes, and hence viral propagation [32]. Therefore, identifying this regulatory switch might be important towards devising specific targets for regulating TAD dimerization and pathogenesis.

Acknowledgment

We thank Mr. Ali Hassan for help in computational modeling, Dr. G. Krishnamoorthy (TIFR, India) for providing the DLS facility and ACTREC for funding the project.

Appendix A. Supplementary data

Supplementary data related to this article can be found at http://dx.doi.org/10.1016/j.bbrc.2015.05.057.

Transparency document

Transparency document related to this article can be found online at http://dx.doi.org/10.1016/j.bbrc.2015.05.057.

References

[1] S.V. Graham, Human papillomavirus: gene expression, regulation and prospects for novel diagnostic methods and antiviral therapies, Future Microbiol. 5 (2010) 1493–1506.
[2] M. Muller, C. Demeret, The HPV E2-host protein-protein interactions: a complex hijacking of the cellular network, Open Virol. J. 6 (2012) 173–189.
[3] A.A. McBride, The papillomavirus E2 proteins, Virology 445 (2013) 57–79.
[4] M. Boulabiar, S. Boubaker, M. Favre, C. Demeret, Keratinocyte sensitization to tumour necrosis factor-induced nuclear factor kappa B activation by the E2 regulatory protein of human papillomaviruses, J. Gen. Virol. 92 (2011) 2422–2427.
[5] S. Blachon, C. Demeret, The regulatory E2 proteins of human genital papillomaviruses are pro-apoptotic, Biochimie 85 (2003) 813–819.
[6] S. Bellanger, S. Blachon, F. Mechali, C. Bonne-Andrea, F. Thierry, High-risk but not low-risk HPV E2 proteins bind to the APC activators Cdh1 and Cdc20 and cause genomic instability, Cell Cycle 4 (2005) 1608–1615.
[7] E.A. Abbate, J.M. Berger, M.R. Botchan, The X-ray structure of the papillomavirus helicase in complex with its molecular matchmaker E2, Genes Dev. 18 (2004) 1981–1996.
[8] C.M. Helfer, R. Wang, J. You, Analysis of the papillomavirus E2 and bromodomain protein Brd4 interaction using bimolecular fluorescence complementation, PLoS One 8 (2013) e77994.
[9] A.A. Antson, J.E. Burns, O.V. Moroz, D.J. Scott, C.M. Sanders, I.B. Bronstein, G.G. Dodson, K.S. Wilson, N.J. Maitland, Structure of the intact transactivation domain of the human papillomavirus E2 protein, Nature 403 (2000) 805–809.
[10] E.A. Abbate, C. Voitenleitner, M.R. Botchan, Structure of the papillomavirus DNA-tethering complex E2:Brd4 and a peptide that ablates HPV chromosomal association, Mol. Cell 24 (2006) 877–889.
[11] H. Rozenberg, D. Rabinovich, F. Frolow, R.S. Hegde, Z. Shakked, Structural code for DNA recognition revealed in crystal structures of papillomavirus E2-DNA targets, Proc. Natl. Acad. Sci. U. S. A. 95 (1998) 15194–15199.
[12] D. Gagnon, H. Senechal, C.M. D'Abramo, J. Alvarez, A.A. McBride, J. Archambault, Genetic analysis of the E2 transactivation domain dimerization interface from bovine papillomavirus type 1, Virology 439 (2013) 132–139.
[13] E.E. Hernandez-Ramon, J.E. Burns, W. Zhang, H.F. Walker, S. Allen, A.A. Antson, N.J. Maitland, Dimerization of the human papillomavirus type 16 E2 N terminus results in DNA looping within the upstream regulatory region, J. Virol. 82 (2008) 4853–4861.
[14] K. Webster, J. Parish, M. Pandya, P.L. Stern, A.R. Clarke, K. Gaston, The human papillomavirus (HPV) 16 E2 protein induces apoptosis in the absence of other HPV proteins and via a p53-dependent pathway, J. Biol. Chem. 275 (2000) 87–94.
[15] S.F. Harris, M.R. Botchan, Crystal structure of the human papillomavirus type 18 E2 activation domain, Science 284 (1999) 1673–1677.
[16] A. Sali, T.L. Blundell, Comparative protein modelling by satisfaction of spatial restraints, J. Mol. Biol. 234 (1993) 779–815.
[17] S.R. Comeau, D.W. Gatchell, S. Vajda, C.J. Camacho, ClusPro: a fully automated algorithm for protein-protein docking, Nucleic Acids Res. 32 (2004) W96–W99.
[18] N. Singh, A. D'Souza, A. Cholleti, G.M. Sastry, K. Bose, Dual regulatory switch confers tighter control on HtrA2 proteolytic activity, FEBS J. 281 (2014) 2456–2470.
[19] R.A. Laskowski, M.W. Macarthur, D.S. Moss, J.M. Thornton, PROCHECK: a program to check the stereochemical quality of protein structures, J. Appl. Cryst. 26 (1993) 283–291.
[20] M. Wiederstein, M.J. Sippl, ProSA-web: interactive web service for the recognition of errors in three-dimensional structures of proteins, Nucleic Acids Res. 35 (2007) W407–W410.
[21] C. Colovos, T.O. Yeates, Verification of protein structures: patterns of nonbonded atomic interactions, Protein Sci. 2 (1993) 1511–1519.
[22] J.E. Burns, O.V. Moroz, A.A. Antson, C.M. Sanders, K.S. Wilson, N.J. Maitland, Expression, crystallization and preliminary X-ray analysis of the E2 transactivation domain from papillomavirus type 16, Acta Crystallogr. D. Biol. Crystallogr. 54 (1998) 1471–1474.
[23] J. Walters, S.L. Milam, A.C. Clark, Practical approaches to protein folding and assembly: spectroscopic strategies in thermodynamics and kinetics, Methods Enzymol. 455 (2009) 1–39.
[24] K.E. Neet, D.E. Timm, Conformational stability of dimeric proteins: quantitative studies by equilibrium denaturation, Protein Sci. 3 (1994) 2167–2174.

[25] Y. Wang, R. Coulombe, D. Cameron, L. Thauvette, M. Massariol, L. Amon, D. Fink, S. Titolo, E. Welchner, C. Yoakim, J. Archambault, P. White, Crystal structure of the E2 transactivation domain of human papillomavirus type 11 bound to a protein interaction inhibitor, J. Biol. Chem. 279 (2004) 6976–6985.
[26] D.O. Alonso, K.A. Dill, Solvent denaturation and stabilization of globular proteins, Biochemistry 30 (1991) 5974–5985.
[27] J.K. Myers, C.N. Pace, J.M. Scholtz, Denaturant m values and heat capacity changes: relation to changes in accessible surface areas of protein unfolding, Protein Sci. 4 (1995) 2138–2148.
[28] J.A. Rumfeldt, C. Galvagnion, K.A. Vassall, E.M. Meiering, Conformational stability and folding mechanisms of dimeric proteins, Prog. Biophys. Mol. Biol. 98 (2008) 61–84.
[29] S. Jones, J.M. Thornton, Protein-protein interactions: a review of protein dimer structures, Prog. Biophys. Mol. Biol. 63 (1995) 31–65.
[30] C.M. Sanders, D. Sizov, P.R. Seavers, M. Ortiz-Lombardia, A.A. Antson, Transcription activator structure reveals redox control of a replication initiation reaction, Nucleic Acids Res. 35 (2007) 3504–3515.
[31] S. Bellanger, C.L. Tan, Y.Z. Xue, S. Teissier, F. Thierry, Tumor suppressor or oncogene? A critical role of the human papillomavirus (HPV) E2 protein in cervical cancer progression, Am. J. Cancer Res. 1 (2011) 373–389.
[32] J. Doorbar, Molecular biology of human papillomavirus infection and cervical cancer, Clin. Sci. (Lond) 110 (2006) 525–541.